1
2
3
4
5
6
7
8
9
10
11
12
13
14
15
16
17
18
19
20
21
22

In-situ quantification of carbonate species concentrations, pH and pCO₂ in calcite fluid

inclusions using confocal Raman spectroscopy.

Michael Naylor Hudgins [a,b,c*], Todd K. Knobbe [a], Julia Hubbard [a], Andrew Steele [d], Justin G.

Park[a,b,c], and Morgan F. Schaller [a,b,c*]

[a] Department of Earth and Environmental Sciences, Rensselaer Polytechnic Institute, Jonsson

Rowland Science Center, Troy, NY, USA

[b] Center for Environmental Stable Isotope Analysis, Rensselaer Polytechnic Institute, Jonsson

Rowland Science Center, Troy, NY, USA

[c] Rensselaer Astrobiology Research and Education Center, Rensselaer Polytechnic Institute,

Jonsson Rowland Science Center, Troy, NY, USA

[d] Earth and Planets Laboratory, Carnegie Institution for Science, Washington, DC, USA

*Corresponding Author: schall@rpi.edu

*Co-corresponding Author: hudgim@rpi.edu

Abstract

Carbonate minerals are globally distributed on the modern and ancient Earth and are abundant in

terrestrial and marine depositional environments. Fluid inclusions hosted by calcite retain

primary signatures of the source fluid geochemistry at the time of mineral formation (i.e., pCO₂)

and can be used to reconstruct paleoenvironments. Confocal laser Raman spectroscopy provides

a quick, non-destructive approach to measuring the constituents of fluid inclusions in carbonates

and is a reliable method for qualitatively determining composition in both the aqueous and gas

phases. Here, we demonstrate a method for accurately quantifying bicarbonate and carbonate ion

concentrations (down to 20 mM) and pH (7-11) from calcite fluid inclusions using confocal

Raman spectroscopy. Instrument calibrations for carbonate (CO_3^{2-}) and bicarbonate (HCO_3^-)

46   concentrations and pH were performed using stock solutions. We show that the calcite host

47   mineral does not affect accurate quantification of carbonate solution concentrations, and that

48   these parameters can be used to estimate the pH and pCO_2 of a solution entrapped within a fluid

49   inclusion. We apply the technique to Icelandic spar calcite and find a $[CO_3^{2-}] = 0.11$, $[HCO_3^-] =$

50   0.17, pH = 10.1, and CO_2 (ppm) = 2217. The presence of gaseous Raman bands for CO_2, CH_4,

51   and H_2S suggests that the mineral precipitated in a reducing environment.

52   **Keywords:** Raman spectroscopy, fluid inclusions, carbonate system, pH, CO_2, quantification

53   **Introduction**

54   Fluid inclusions provide a wealth of information pertaining to a mineral's environment at

55   the time of formation.[1,2] The ability to quantify the constituents within fluid inclusions provides

56   information on geochemical parameters such as initial temperature and pressure conditions,

57   salinity, pH, and solution and gas composition of any included gas phases.[3–9] These geochemical

58   indicators can be estimated by using Raman spectroscopy, a non-destructive method, that can be

59   applied to the in-situ study of micron-scale fluid inclusions.[6,10–14]

60   Calcium carbonate minerals are common and abundant in a variety of environmental

61   settings on Earth, ranging from metamorphic carbonates forming in subduction zones to low

62   temperature authigenic marine sediments and surficial deposits (pedogenic or speleothems).[14–17]

63   Many of these types of carbonates contain fluid inclusions; metamorphic carbonates have been

64   used to track carbon transport in Earth's interior, and low-temperature carbonate fluid inclusions

65   have been used as paleoenvironmental proxies in both the terrestrial and marine realms.[15–18]

66   Many studies have focused on carbon and oxygen isotopic compositions of either the mineral

67   matrix or fluid within inclusions, but relatively fewer studies have investigated the gas

68   concentration or aqueous composition of fluid inclusions in non-diagenetic carbonate minerals.

69   [15–21]

70   A fundamental problem in paleoclimatology is the lack of accurate atmospheric pCO_2

71   estimates prior to the ice core record.[22,23] The proxy methods that have been deployed (e.g., the

72    $\delta^{13}C$ of pedogenic carbonates, leaf stomatal indices, and boron isotopes) show similar trends but

73   disagree in absolute value.[16,24–30] However, dissolved gases and solutes in the aqueous phase of

74   carbonate mineral fluid inclusions can provide valuable insight into the geochemical conditions

75   of the mineral's formation environment, which can be related back to absolute atmospheric

76   concentrations at the time of precipitation.[1–4,7,31] Unfortunately, these techniques require the

77   destruction of fluid inclusions during bulk analyses of the released gases and require large

78   sample sizes to enable accurate measurement.[32–34] In contrast, Raman spectroscopy is a non-

79   destructive method that can provide analyses of liquid and gas phase compositions within

80   individual fluid inclusions.[5,35] This method enables each of the components of the carbonate

81   system (e.g., $[CO_3^{2-}]$, $[HCO_3^-]$, pH, and pCO_2) to be quantified discretely in-situ without

82   disturbing the host mineral matrix. However, before quantification of any molecules measured

83   directly within natural fluid inclusion samples, the mineral system's Raman spectrum and the

84   host mineral's effects on solute quantification need to be evaluated.

85   Identification and quantification of the carbonate species (e.g., CO_3^{2-}, HCO_3^-)

86   concentration provides information on solution pH and pCO_2 of the system that the mineral

87   precipitated in.[36] In moderately alkaline systems, HCO_3^- is the dominant carbon species in

88   solution, and the Raman signal of HCO_3^- has been observed in alkaline solutions in quartz hosted

89   fluid inclusions.[14,37,38] However, these studies only recorded the presence of HCO_3^- and did not

90   attempt to quantify the concentration. Although a weak Raman scatterer, detailed studies have

91   shown that HCO_3^- is amenable to quantification over a range of concentrations using Raman

92   spectroscopy.[39–41] However, these studies did not address the applicability of Raman

93   spectroscopy to quantifying HCO_3^- concentrations in natural samples.

94   In this study, we present a method for the accurate measurement of $[CO_3^{2-}]$ and $[HCO_3^-]$

95   in fluid inclusions via Raman spectroscopy and use these measurements to estimate the pH and

96   pCO_2 with which the inclusion fluid had equilibrated. We construct calibration curves for CO_3^{2-},

97   HCO_3^-, and pH using Na_2CO_3 and $NaHCO_3$ solutions via two different methods (with and

98   without the addition of a calcite cover slip to examine the effects of the host mineral), with the

99   ultimate goal of applying these calibrations to natural carbonate samples.[42] We then evaluate the

100 accuracy of each method for determining the concentration of CO_3^{2-} and HCO_3^- in natural fluid

101 inclusions. We also investigate the effect of increasing solution salinity on the quantification of

102 solutes in fluid inclusions. These studies reveal that $[CO_3^{2-}]$, $[HCO_3^-]$, pH, and pCO_2 of alkaline

103 solutions can be determined using the main Raman bands for CO_3^{2-} and HCO_3^-. The approaches

104 and methods developed in this paper can be applied to a range of fluid inclusions at 1 atm. The

105 specific effects of temperature and pressure broadening on Raman band parameters of $[CO_3^{2-}]$,

106 $[HCO_3^-]$ are not addressed in this study and have been investigated elsewhere.[43,44]

107

108 **Methods**

109 *Calibration Solutions*

110   Prior Raman calibration studies for CO_3^{2-} and HCO_3^- in solution have been made at

111 concentrations spanning from dilute solutions to near saturation ($[HCO_3^-]$: 0.63-0.0004 molar;

112 $[CO_3^{2-}]$: 0.49-0.0002 molar).[39,41,45] Here, we focus on calibrating the Raman response to CO_3^{2-}

113 and HCO_3^- concentrations in dilute carbonate solutions that are closer to those observed in

5

114   natural systems (Table I). We prepared solutions of Na_2CO_3 and $NaHCO_3$ over a range of $[CO_3^{2-}$

115   ], $[HCO_3^-]$, and pH that represent observed concentrations of natural systems (Table I and

116   II).[36,46–52] Natural fluid inclusions in carbonates forming at the surface and in seawater have a

117   range of salinities.[3] Therefore, we also constructed calibrations over a range of NaCl salinities

118   (0-20 wt%) to more closely resemble natural systems and to investigate salinity effects on the

119   Raman band response of carbonate species and pH quantification. We consider NaCl calibrations

120   necessary because previous studies have demonstrated that increasing salinity alters the

121   dissociation and solubility constants (K_{co2}, K_1, and K_2) and skews the OH^- stretch of H_2O, thus

122   potentially leading to an inaccurate estimation of carbonate species concentrations where

123   freshwater calibration curves are applied to saline inclusions.[8,53,54]

124   A portion of solutions were equilibrated with the atmosphere and the remainder were

125   prepared as a close system, to encompass a full range of relevant carbonate species

126   concentrations. Desired weights of $NaHCO_3$, Na_2CO_3, and NaCl were placed in 50 mL centrifuge

127   tubes and continuously mixed with 50 mL of Millipore water (18 Ω) until fully dissolved. Open

128   system solutions were mixed until atmospheric equilibrium was reached. To obtain a pH <8, 1.2

129   molar HCl (10% HCl by volume) was added to a 0.25 molar $NaHCO_3$ solution. Once the acid

130   was added, the solution was mixed until a stable pH was achieved. Solution temperature and pH

131   were measured with a Thermo Scientific Orion 2-star pH meter before spectroscopic

132   measurement.

133   To calculate the amount of HCO_3^- and CO_3^{2-} in the closed system solutions at the time of

134   measurement, the initial amount of HCO_3^- and CO_3^{2-} mixed in the solution was assumed to be

135   equal to the total dissolved inorganic carbon (TDIC). Aqueous speciation of the closed carbonate

136   system was calculated based on measured temperature and pH using the following equations (Eq.

137   1 and 2):[55]

$$[HCO_3^-] = C_T \frac{K_1[H^+]}{[H^+]^2 + K_1[H^+] + K_1 K_2} \qquad (1)$$

$$[CO_3^{2-}] = C_T \frac{K_1 K_2}{[H^+]^2 + K_1[H^+] + K_1 K_2} \qquad (2)$$

140   Where $[HCO_3^-]$ is molar HCO_3^-; $[CO_3^{2-}]$ is molar CO_3^{2-}; C_T is molar TDIC (the initial

141   amount of HCO_3^- and CO_3^{2-} put into solution as a $NaHCO_3$ and Na_2CO_3 salt; K_1 and K_2 are

142   temperature-dependent equilibrium constants that account for the dissociation of H_2CO_3 and

143   HCO_3^-, respectively; and $[H^+]$ is molar hydrogen ions.

144   For solutions prepared as an open system, HCO_3^- and CO_3^{2-} concentrations were

145   calculated based on the open system equations:[56]

$$[HCO_3^-] = \frac{K_1 K_{co2} pCO_2}{[H^+]} \qquad (3)$$

$$[CO_3^{2-}] = \frac{K_1 K_2 K_{co2} pCO_2}{[H^+]^2} \qquad (4)$$

148   K_{CO2} (i.e., Henry's constant) is the temperature-dependent equilibrium constant that

149   accounts for the aqueous solubility of CO_2. When estimating carbonate species concentrations

150   for the calibrations, the equilibrium constants were adjusted to the measured temperature values

151   using the calculations of Drever (1997).[56]

152   We used the closed system calculations to estimate pCO_2 in natural fluid inclusions

153   because the trapped solute acts as a closed system post-entrapment and the components of the

154   fluid (alkalinity, TDIC, pH, and pCO_2) are fixed. However, the fluid inclusion would represent

155   the environment pre-entrapment as the solute was equilibrated with the atmosphere, assuming

7

156   the mineral formed at the Earth's surface. Therefore, fluid inclusions behave as a closed system

157   and estimations of pCO_2 should use such equations.

158   Closed system estimations of pCO_2 require information on $[CO_3^{2-}]$, $[HCO_3^-]$, $[CO_{2\ aq}]$,

159   and pH. Our calibrations can quantify $[CO_3^{2-}]$ and $[HCO_3^-]$, but pH must be calculated from the

160   former, as does $[CO_{2\ aq}]$ because its concentration is low in the natural range chosen in this study

161   (Table II).[55] To estimate pH, we use the following equation:

$$[H^+] = \frac{[HCO_3^-]K_2}{[CO_3^{2-}]} \tag{5}$$

163   And $[CO_{2\ aq}]$ was calculated by the following equation:

$$[CO_{2\ aq}] = [H^+]^2 \frac{[CO_3^{2-}]}{K_1 K_2} \tag{6}$$

165   Which allows for pCO_2 to be estimated from the calculated $[CO_{2\ aq}]$:

$$pCO_2 = \frac{[CO_{2\ aq}]}{K_{co2}} \tag{7}$$

167   To ensure that calibration solutions capture a large range of hypothetical pCO_2 values, we

168   calculated pCO_2 from all the calibration solutions using the closed system (Eq. 5, 6, and 7) (Fig.

169   1). These calculations show that the calibration solutions can be used to estimate a wide range of

170   pCO_2 (10 to 10^5 ppm of CO_2) values (Fig. 1).

171

172   *Evaluating the Effect of the Carbonate Host Mineral*

173   To evaluate whether birefringence of the host mineral effects the calibration curves of

174   solute concentrations in a natural carbonate sample, a cover slip was made from optical grade

175   calcite to simulate the measurement of a calcite-hosted fluid inclusion. Previous research has

176   demonstrated that the host mineral does not affect determination of salt concentrations in calcite

8

177   when using a confocal Raman Spectrometer.[8,42] Those authors suggest minimizing the effect of

178   the host mineral in Raman spectroscopy micro-fluid inclusion studies by placing the sample at its

179   extinction position. To test this, a piece of optical grade calcite that has the c-axis parallel to

180   surface and free of visible inclusions and defects was used in a subset of measurements to ensure

181   the host mineral does not affect solute quantification. The cover slip was ground to a thickness of

182   ~100 microns and doubly polished to a colloidal silica grade.

183   A comparison of the standard $NaHCO_3$ and Na_2CO_3 solutions measured by Raman both

184   with and without the addition of a calcite cover slip was performed for each concentration to

185   measure the effect of the host mineral on solute quantification (Fig. 2). To ensure that the desired

186   focal plane was in the solution, before each measurement, the laser was first focused on the

187   surface of the cover slip and then focused down to the underside of the cover slip, and finally

188   focused 100 microns below and into the solution. For solutions without the calcite cover slip, the

189   laser was focused 100 microns below the surface of the solution.

190

191   *Raman Measurement and quantification of CO_3^{2-} and HCO_3^-*

192   Shortly after a solution was mixed and the open system solutions reached equilibrium, 5

193   microliters of solution were placed in a glass concavity slide and analyzed using a WiTec

194   alpha300 R confocal Raman spectrometer utilizing a 532 nm green laser at the Carnegie Institute

195   of Science, Earth and Planets Laboratory.[57] Laser power at the source was 14 mW during each

196   analysis. Measurements were made using a Zeiss 50x objective, a 50 μm aperture, and a 1 cm^{-1}

197   spectral resolution using a Witec UHTS spectrometer system with a 600 grating and an Andor

198   DV400 camera cooled to -59 °C. Additional measurements were made on a Bruker SENTERRA

199   Raman spectrometer at Rensselaer Polytechnic Institute, Department of Earth and Environmental

9

200 Science. Measurements were integrated for 30 seconds with 3 accumulations and alternated

201 between the solution and the solution with calcite cover slip to minimize any evolution in the

202 solution composition over the course of the analyses. Each component (H_2O, HCO_3^-, and CO_3^{2-}

203 solution with and without the calcite cover slip, and the calcite cover slip alone) used in this

204 study can be broken down into their individual Raman spectra (i.e., H_2O, $CaCO_3$, etc. measured

205 independently), and when constructed together, form a spectra that simulates a fluid inclusion

206 (Fig. 2).

207   The HCO_3^- anion has a weak Raman scatter, but in alkaline solutions, HCO_3^- is the

208 dominant anion of the carbonate system and has 9 normal, partially polarized Raman

209 modes.[5,41,58] The two broad, weak bands at 634 cm^{-1} and 673 cm^{-1} with the latter representing

210 $\delta CO2$. The broad mode at 634 cm^{-1} can be deconvoluted into three sub-bands at 630 cm^{-1}, 634

211 cm^{-1}, and 640 cm^{-1} to represent γCO-H and δHOC. HCO_3^- modes are prevalent at 843 cm^{-1}

212 (γCO_3), 1017 cm^{-1} (νC-OH), 1312 cm^{-1} (δCO-H), 1360 cm^{-1} ($\nu_s CO_2$), 1630 cm^{-1} ($\nu_{as} CO_2$), and

213 2600 cm^{-1} (νCO-H)[41]. CO_3^{2-} has 6 active Raman bands, where weak bands occur at 684 cm^{-1} (ν_4,

214 in-plane deformation), 885 cm^{-1} (ν_2, out-of-plane deformation), 1385 cm^{-1} (ν_3, antisymmetric

215 stretch C-O), 1435 cm^{-1}, and 1764 cm^{-1} and a strong band at 1066 cm^{-1} (ν_1, C-O symmetric

216 stretch).[5,39,41] Calcite has 5 active Raman bands, where weak bands occur at 156 (T,

217 translational), 711 (ν_4, in-plane deformation), 1435 (ν_3, antisymmetric stretch), and strong bands

218 occur at 284 (T, translational) and 1088 (ν_1, symmetric stretch).[5] However, to avoid issues with

219 band interferences, low intensity signals, and/or mineral fluorescence, the main vibrational mode

220 of HCO_3^- at 1017 cm^{-1} and CO_3^{2-} at 1066 cm^{-1} was used to quantify the amount of [HCO_3^-] and

221 [CO_3^{2-}] in solutions as these are the strongest bands.[5,41]

222   Calibration solution data was exported in OriginLab (OriginLab Corp., Northampton,

223   MA, USA) where the spectra was background subtracted and the main HCO_3^- and CO_3^{2-} bands

224   were integrated for their cumulative area (A_{HCO3-} and A_{CO32-}). The area of the HCO_3^- and CO_3^{2-}

225   bands were normalized to the water band (e.g., A_{CO32-}/A_{H2O}) as this parameter acts as a reliable

226   internal standard (Fig. 1).[45] The areas of the HCO_3^- and CO_3^{2-} bands were ratioed (A_{CO32-}/A_{HCO3-})

227   as this parameter is reliable in estimating pH, since the carbonate species concentrations are pH

228   dependent.

229   The ratioed area of the bands and the calculated $[HCO_3^-]$ and $[CO_3^{2-}]$ of calibration

230   solutions are used to build calibration curves which allows us to estimate $[CO_3^{2-}]$, $[HCO_3^-]$, and

231   pH, and ultimately pCO_2, in an unknown sample.[39,59] Solution calibrations were also constructed

232   over a range of NaCl salinities (0-20 wt%) to resemble natural systems and evaluate the effects

233   of NaCl on the OH^- stretch of H_2O and the carbonate species Raman bands. The data collected

234   from the Carnegie Institute for Science's and Rensselaer Polytechnic Institute's confocal Raman

235   spectrometers show that the $[CO_3^{2-}]$, $[HCO_3^-]$, and pH solution curves have considerable overlap

236   and have a near 1:1 agreement with each other (Fig. 3). The small offset between the two

237   instruments may be due to differences in laser output, but this comparison clearly demonstrates

238   that our calibration method is largely independent of the specifics of the instrumentation.

239

240   *Optical Calcite Fluid Inclusion*

241   An Icelandic Spar calcite sample of an unknown origin was used to evaluate the

242   applicability of our calibration's curves to natural carbonate samples. The Icelandic Spar calcite

243   was chosen as a proof of concept, as it contains an abundance of large primary fluid inclusions.

244   An inclusion-free portion of the same mineral was used to make the calcite cover slip and

245   provides the best matrix matched sample to test the calibration curves. The fluid inclusions in the

246   Icelandic Spar calcite are predominantly of two phases, vapor and liquid. For demonstration of

247   the success of the calibration technique, a large inclusion ~150 μm across and ~150 μm below

248   the sample surface was analyzed. Measurements were focused on this inclusion because the area

249   of the phases (aqueous or vapor) of interest were substantially larger than the laser spot size (~1

250   μm or less). Fluorescence from the host calcite makes it increasingly difficult to analyze small

251   inclusions, especially as parameters such as integration time and accumulations are increased. If

252   the concentrations of the carbonate species in solution are quantified, then the pH and pCO_2 can

253   be determined in a fluid inclusion using equations five and seven.[55] The spectra of the Icelandic

254   Spar calcite were processed and deconvoluted as the calibration solution, as described in the

255   previous section.

256

257   **Results and Discussion**

258   *Calibration Curves*

259   Area ratio calibrations for standard solutions (without NaCl) with and without the calcite

260   cover slip are similar (Fig. 3 and Table III; consult this table for equations). Quantification of

261    $[CO_3^{2-}]$ and $[HCO_3^-]$ using A_{CO32-}/A_{H2O-} and A_{HCO3-}/A_{H2O} show a linear relationship, respectively,

262   with and without the calcite cover slip (Fig. 3). Calibration curves for $[CO_3^{2-}]$ show linear

263   relationships with increasing salinities (0-20 wt% NaCl) and the increasing saline calibration

264   solutions have similar slopes and intercepts (Fig. 4). This is likely due to K_1 and K_2 equilibrium

265   constants being limited to salinities <45.[53] The fresh and saline calibration curves for $[HCO_3^-]$

266   show linear relationships with similar slopes and intercepts (Fig. 4 and Table IV; consult this

267   table for equations). Quantification of pH using A_{CO32-}/A_{HCO3-} shows a linear relationship when

12

268   the area ratio is logarithmically scaled, with and without the calcite cover slip (Fig. 3). The linear

269   saline solution calibration curves for pH display a spreading pattern with increasing salinity. The

270   limit of quantification and detection are 0.0001 and 0.00005 for $A_{HCO_3^-}/A_{H_2O}$, 0.0002 and

271   0.00008 for $A_{CO_3^{2-}}/A_{H_2O}$, and 0.23 and 0.08 for $A_{CO_3^{2-}}/A_{HCO_3^-}$. The equation used for LOQ is

272    $LOQ = 10\frac{\sigma}{s}$ and LOD is $LOD = 3.3\frac{\sigma}{s}$, where σ is the standard deviation of the response and s is

273   the slope of the calibration curve. The solution calibration curves produced in this study are

274   robust as these measurements can be made equally on two interlaboratory confocal Raman

275   spectrometers (Fig. 3).

276

277   *Characterization of the Raman spectra*

278   The solutions with the calcite cover slip have a band at 1088 cm^{-1} that may interfere with

279   CO_3^{2-} in solution and can pose a potential problem in accurately quantifying carbonate species at

280   low concentrations in fluid inclusions, as discussed in Dubessy et al.[12] However, the confocal

281   Raman spectrometer also detects a low $CaCO_3$ band at 1088 cm^{-1} that does not interfere with the

282   CO_3^{2-} signal (Fig. 2). With this, the calcite cover slip has little to no effect on estimating $[CO_3^{2-}]$

283   and $[HCO_3^-]$ of the system when using carbonate species areas ratioed to the water peak. At

284   lower concentrations, HCO_3^- and CO_3^{2-} becomes harder to distinguish from the background (pH

285   = <7) and perhaps an additional extrapolation scheme may be needed.

286   Caumon et al.[42] demonstrated that if the crystal symmetry and optical properties are not

287   accounted for then quantification errors can occur. However, this is not a concern in our analyses

288   because we employ a confocal Raman spectrometer which bypasses the calcite cover slip as it is

289   above the focal point and does not contribute to the analysis.[35,60] Given this, there is no

290   substantial difference expected, and accordingly little effect is observed on the calibration curves

13

291   between non- and calcite cover slip analyses (Fig. 3). The confidence intervals indicate no major

292   differences between non-calcite cover slip and calcite cover slip as they overlap one another

293   (Fig. 3 and Table III).

294   Accounting for salinity in estimating $[HCO_3^-]$ is likely minor at all concentrations as the

295   slope of the calibrations for different salinities overlap within their respective confidence

296   intervals (Fig. 4 and Table IV). Therefore, it may be unnecessary to account for the effects of

297   salinity for a solution at low concentrations (e.g., seawater) and pH in natural fluid inclusions.

298   However, salinity should be taken into consideration when estimating $[CO_3^{2-}]$ as the carbonate

299   ion concentration is greatly affected at the lowest NaCl wt% (Fig. 4). Mernagh and Wilde[6] and

300   Sun et al.[8] demonstrated that the OH^- Raman stretch can be used to quantify NaCl concentration

301   of a fluid inclusion, and their methods can be applied to the natural fluid inclusion to determine

302   NaCl concentration, allowing for accurate $[CO_3^{2-}]$ and $[HCO_3^-]$ estimations using our

303   calibrations.[6,8] Overall, the relationships observed are a promising approach towards accurately

304   quantifying carbonate species to estimate pH and pCO_2 in natural samples.

305

306   Measurement of fluid inclusion in Calcite

307   The results of measurements of the aqueous and gaseous phases of a ~150 micron fluid

308   inclusion in the Icelandic Spar calcite are shown in Figure 5. The inclusion formed in an area of

309   the crystal that showed no signs of fracture healing or continual mineral growth along a growth

310   plane.[61] Because the origin, internal pressure, density, and temperature of formation of the fluid

311   inclusion are unknown, this section and the measurements described within are presented as a

312   demonstrative proof of concept. We chose this sample for its ample size and ease of

313   measurement. Within these constraints, the density of the gaseous phase CO_2 can be determined

314   by using the Fermi diad band difference (v_1-$2v_2$) of CO_2.[62,63] It is worth noting that although fluid

315   inclusion homogenization experiments can be used to determine temperature of formation, it is

316   beyond the scope of this study.

317   In the aqueous phase spectra, the distinctive bands of the calcite host mineral can be

318   observed as well as a HCO_3^- and CO_3^{2-} band at 1017 cm^{-1} and 1066 cm^{-1}, respectively (Fig. 5).

319   The OH^- stretch is present between 2750-3700 cm^{-1}. The salinity in the fluid inclusion was

320   estimated to be 19.9 wt% using the equation of Wang et al.[64], assuming that NaCl only is present

321   in solution. The areas between the HCO_3^- and CO_3^{2-} bands were calculated, ratioed against the

322   water band, and applied to the calibration curves without the calcite cover slip. Using equation

323   five, pH was estimated to be 10.1 ± 0.19, and $[HCO_3^-]$ and $[CO_3^{2-}]$ were determined to be $0.17 \pm$

324   0.05 and 0.11 ± 0.03 molar, respectively (Table V). The dissociation and solubility constants

325   were adjusted to the measured salinity value using the calculations of Millero[53] and Onda et al.[54]

326    $25C^o$ was assumed for the solubility and dissociation constants to calculate pCO_2 because the

327   temperature at the time of formation is unknown. With carbonate concentrations, alkalinity, and

328   solution pH estimated, pCO_2 was calculated to be -2.75 ± 0.29 (2217 ± 1319 ppm).

329   In the gaseous phase spectra, the CO_2 Fermi diad is present at 1287 cm^{-1} and 1389 cm^{-1},

330   hydrogen sulfide and methane are also present at 2611 cm^{-1} and 2917 cm^{-1}, respectively (Fig. 5).[5]

331   This suggests that the fluid inclusion formed in an atmosphere below 0.1 g/cm^3 of CO_2, which is

332   the lower limit of the fermi diad calibration.[62,63] However, the density of CO_2 in the present-day

333   atmosphere is 0.0019 g/cm^3, two orders of magnitude below the lowest calibration point. In

334   addition, the lack of major atmospheric gases (e.g., O_2 and N_2), the presence of H_2S and CH_4

335   suggest that the fluid inclusion precipitated in a reducing environment.

336

337 *Calibration Limitations*

338   Quantification of $[CO_3^{2-}]$ and $[HCO_3^-]$ can provide information about the pH and pCO_2 of

339 formation of a carbonate fluid inclusion, and there is no observed effect from the host mineral on

340 estimating pCO_2, pH, and carbonate species when using a confocal instrument (Fig. 3).[8,42]

341 However, there are limitations using this method, including: (1) the Raman spectrometer was

342 calibrated at low temperatures and pressures (1 atm), where it is likely the calibrations will

343 deviate at higher temperatures and pressures as the solubilities and the dissociation constants of

344 the carbonate species change.[65,66] (2) The calibrated Raman spectrometer does not encompass the

345 low pH range present in modern and ancient systems (e.g., acidic springs and soils).[46,48,52] (3)

346 Determining the alkalinity of fluid inclusions may be impossible with current technology as

347 titrating them would lead to fluid contamination. However, it is reasonable to assume that the

348 alkalinity would be controlled by the carbonate system, as it is in the modern oceans.[67] (4) Salts

349 (e.g., $MgCl_2$, $CaCl_2$, and KCl) are likely to be present in natural carbonate fluid inclusions that

350 will skew the water bands and may affect accurate determination of pH and species

351 concentrations.[8,64] (5) Analyses of fluid inclusions are based on small amounts of solution, and

352 this limits the determination of carbonate species concentrations and pH, as a relationship exists

353 between the intensity and the number of molecules present in the sample.[68] For example, if there

354 is a limited amount of water in a carbonate fluid inclusion, a lower intensity water band will be

355 observed, and as a consequence of this, the HCO_3^- and CO_3^{2-} bands may not be detectable in

356 these inclusions. However, larger carbonate fluid inclusions are promising as more solution is

357 present and may be able to detect HCO_3^- and CO_3^{2-} (Fig. 5).

358

359 *Other Applications*

360   The different proxies to estimate pCO_2 in deep time do not agree with one another.[16,24–26]

361   For example, data from $\delta^{13}C$ of paleosol carbonates and stomatal indices of fossil plants from the

362   end-Triassic extinction show a corroborating pCO_2 trend, but the absolute pCO_2 values do not

363   agree.[27–29] One reason is the soil productivity parameter (S(z)) within the soil diffusion model.[26]

364   This parameter is the concentration of CO_2 in the soil derived from the respiration of organic

365   matter and CO_2 in the atmosphere. CO_2 estimations within a soil are largely unknown and

366   unconstrained because this parameter will fluctuate depending on soil profile depth and soil

367   type.[16] However, the calibration presented in this study is a potential method that can constrain

368   the S(z) and estimate pCO_2 within a soil column.

369

370   **Conclusion**

371   We demonstrate the calibration of a confocal Raman spectrometer over a range of $[CO_3^{2-}]$

372   and $[HCO_3^-]$, representative of natural waters. These calibrations allow for the quantification of

373   carbonate species concentrations in fluid inclusion at low-temperatures and pressures.

374   Calibrations can be used to calculate $[CO_3^{2-}]$ and $[HCO_3^-]$, which ultimately allows pH and pCO_2

375   to be determined in mineral fluid inclusions, assuming the mineral formed at the Earth's surface

376   and equilibrated with its environment. The host mineral's crystal optics have little to no effect on

377   determining the $[CO_3^{2-}]$ and $[HCO_3^-]$ if the Raman spectrometer is confocal. Homogenization

378   temperature experiments should be conducted in conjunction with confocal Raman experiments

379   to determine accurate pH and pCO_2 estimations in natural fluid inclusions.

380

17

388

Declaration of Conflicting Interest

391

References

393   1.   R.H. Goldstein. "Clues from Fluid Inclusions". Science. 2001. 294(5544): 1009–1011.

394   2.   E. Roedder. "Introduction to Fluid Inclusions". MSA. 1984. 12: 1–10.

395   3.   R.J. Bodnar. "Introduction to Aqueous-Electrolyte Fluid Inclusions". In: I. Samson, A.

396   Anderson, D. Marshall, editors. Fluid Inclusions: Analysis and Interpretation. Mineral.

397   Assoc. Canada, Quebec City, QC, 2003. Vol. 32. Chap. 4. Pp. 81-99.

398   4.   L.W. Diamond. "Systematics of H_2O Inclusions". In: I. Samson, A. Anderson, D.

399   Marshall. Fluid Inclusions: Analysis and Interpretation. Quebec: Mineral. Assoc. Canada,

400   2003. Vol. 32. Chap. 3. 55-80.

401   5.   M.L. Frezzotti, F. Tecce, A. Casagli. "Raman Spectroscopy for Fluid Inclusion Analysis".

402   J. Geochem. Explor. 2012. 112: 1–20.

403   6.   T.P. Mernagh, A.R. Wilde. "The Use of the Laser Raman Microprobe for the

404   Determination of Salinity in Fluid Inclusions". GCA. 1989. 53(4): 765–771.

405   7.   T.K. Lowenstein, M.N. Timofeeff, S.T. Brennan, L.A. Hardie, R.V. Demicco.

406   "Oscillations in Phanerozoic Seawater Chemistry: Evidence from Fluid Inclusions".

407   Science. 2001. 294(5544): 1086–1088.

408   8.   Q. Sun, L. Zhao, N. Li, J. Liu. "Raman Spectroscopic Study for the Determination of Cl^-

409   Concentration (Molarity Scale) in Aqueous Solutions: Application to Fluid Inclusions".

410   Chem. Geol. 2010. 272(1–4): 55–61.

411   9.   T. Azbej, M.J. Severs, B.G. Rusk, R.J. Bodnar. "In situ Quantitative Analysis of Individual

412   H_2O–CO_2 Fluid Inclusions by Laser Raman Spectroscopy". Chem. Geol. 2007. 237(3–4):

413   255–263.

414   10. B. Wopenka, J.D. Pasteris. "Raman Intensities and Detection Limits of Geochemically

415   Relevant Gas Mixtures for a Laser Raman Microprobe". Anal. Chem. 1987. 59(17): 2165–

416   2170.

417   11. J. Dubessy, B. Poty, C. Ramboz. "Advances in C-O-H-N-S Fluid Geochemistry based on

418   Micro-Raman spectrometric Analysis of Fluid Inclusions". EJM. 1989. 1(4): 517–534.

419   12. J. Dubessy, M.-C. Boiron, A. Moissette, C. Monnin, N. Sretenskaya. "Determination of

420   Water, Hydrates and pH in Fluid Inclusions by Micro-Raman Spectrometry". EJM. 1992.

421   4: 885–894.

422   13. E.A.J. Burke. "Raman Microspectrometry of Fluid Inclusions". Lithos. 2001. 55(1): 139–

423   158.

424   14. M.L. Frezzotti, J. Selverstone, Z.D. Sharp, R. Compagnoni. "Carbonate Dissolution

425   during Subduction revealed by Diamond-bearing Rocks from the Alps". Nature Geosci.

426   2011. 4(10): 703–706.

427 15. U. Brand, N. Blamey, C. Garbelli, E. Griesshaber, R. Posenato, L. Angiolini, et al.

428   "Methane Hydrate: Killer cause of Earth's Greatest Mass Extinction". Palaeoworld. 2016.

429   25(4): 496–507.

430 16. T.E. Cerling. "Stable Carbon Isotopes in Palaeosol Carbonates". In: M. Thiry, R. Simon-

431   Coinçon, editors. Palaeoweathering, Palaeosurfaces and Related Continental Deposits.

432   Blackwell Publishing Ltd., Oxford, UK, 2009. Pp. 43–60.

433 17. M.L. Griffiths, R.N. Drysdale, H.B. Vonhof, M.K. Gagan, J. Zhao, L.K. Ayliffe, et al.

434   "Younger Dryas–Holocene Temperature and Rainfall History of Southern Indonesia from

435   $\delta^{18}O$ in Speleothem Calcite and Fluid Inclusions". Earth Planet. Sci. Lett. 2010. 295(1):

436   30–36.

437 18. N. Tabor, T. Myers. "Paleosols as Indicators of Paleoenvironment and Paleoclimate".

438   Annu. Rev. Earth and Planet. Sci. 2014. 43: 150317182938004.

439 19. H.P. Schwarcz, R.S. Harmon, P. Thompson, D.C. Ford. "Stable Isotope Studies of Fluid

440   Inclusions in Speleothems and their Paleoclimatic Significance". GCA. 1976. 40(6): 657–

441   665.

442 20. K. Azmy, N.J.F. Blamey. "Source of Diagenetic Fluids from Fluid-Inclusion Gas Ratios".

443   Chem. Geol. 2013. 347: 246–254.

444 21. N. Blamey, P. Boston, L. Rosales-Lagarde. "High-Resolution Signatures of Oxygenation

445   and Microbiological Activity in Speleothem Fluid Inclusions". IJS. 2016. 45(3): 231–241.

446 22. D. Lüthi, M. Le Floch, B. Bereiter, T. Blunier, J.-M. Barnola, U. Siegenthaler, et al.

447   "High-Resolution Carbon Dioxide Concentration Record 650,000–800,000 Years Before

448   Present". Nature. 2008. 453(7193): 379–382.

449   23. The Cenozoic CO Proxy Integration Project (CenCOPIP) Consortium*†, B. Hönisch, D.L.

450   Royer, D.O. Breecker, P.J. Polissar, G.J. Bowen, et al. "Toward a Cenozoic History of

451   Atmospheric CO_2". Science. 2023. 382(6675): eadi5177.

452   24. D.L. Royer, K.M. Moynihan, M.L. McKee, L. Londoño, P.J. Franks. "Sensitivity of a Leaf

453   Gas-Exchange Model for Estimating Paleoatmospheric CO_2 Concentration". Clim. Past.

454   2019. 15(2): 795–809.

455   25. S.M. Eggins, L.L. Haynes, K.A. Allen, K.D. Holland, K. Lorbacher, B. Hönisch. Boron

456   Proxies in Paleoceanography and Paleoclimatology. 1st edition. Wiley-Blackwell,

457   Hoboken, NJ, 2019.

458   26. D.O. Breecker. "Quantifying and Understanding the Uncertainty of Atmospheric CO_2

459   Concentrations Determined from Calcic Paleosols". Geochem. geophys. 2013. 14(8):

460   3210–3220.

461   27. M.F. Schaller, J.D. Wright, D.V. Kent. "Atmospheric pCO_2 Perturbations Associated with

462   the Central Atlantic Magmatic Province". Science. 2011. 331(6023): 1404–1409.

463   28. M.F. Schaller, J.D. Wright, D.V. Kent, P.E. Olsen. "Rapid emplacement of the Central

464   Atlantic Magmatic Province as a Net Sink for CO_2". Earth Planet. Sci. Lett. 2012. 323–

465   324: 27–39.

466   29. J.C. McElwain, D.J. Beerling, F.I. Woodward. "Fossil Plants and Global Warming at the

467   Triassic-Jurassic Boundary". Science. 1999. 285(5432): 1386–1390.

468   30. M.F. Schaller, J.D. Wright, D.V. Kent. "A 30 Myr Record of Late Triassic Atmospheric

469   pCO_2 Variation Reflects a Fundamental Control of the Carbon Cycle by Changes in

470   Continental Weathering". Geol. Soc. Am. Bull. 2015. 127(5–6): 661–671.

471   31. L.W. Diamond. "Review of the Systematics of CO_2–H_2O Fluid Inclusions". Lithos. 2001.

472   55(1–4): 69–99.

473   32. J.L. Zimmermann, R. Moretto. "Release of Water and Gases from Halite Crystals". EJM.

474   1996. 8(2): 413–422.

475   33. D.I. Norman, N. Blamey, J.N. Moore. "Interpreting Geothermal Process and Fluid

476   Sources from Fluid Inclusion Organic Compounds and CO_2/N_2 Ratios". Twenty-Seventh

477   Workshop on Geothermal Reservoir Engineering. 2002.

478   34. A.E. Williams. "Mass Spectrometric Analysis of Volatiles in Fluid Inclusions: Aliquot

479   Calibration Valve to Simulate Inclusion Rupture". Chem. Geol. 1996. 131(1): 155–165.

480   35. M. Fries, A. Steele. "Raman Spectroscopy and Confocal Raman Imaging in Mineralogy

481   and Petrography". In: J. Toporski, T. Dieing, O. Hollricher. Confocal Raman Microscopy.

482   New York, NY: Springer Link, 2011. Chap. 3. Pp. 209–236.

483   36. J.N. Butler. Carbon Dioxide Equilibria and their Applications. Routledge, New York,

484   1982. Pp. 1-259.

485   37. T. Hrstka, J. Dubessy, J. Zachariáš. "Bicarbonate-Rich Fluid Inclusions and Hydrogen

486   Diffusion in Quartz from the Libčice Orogenic Gold Deposit, Bohemian Massif". Chem.

487   Geol. 2011. 281(3–4): 317–332.

488   38. S. Facq, I. Daniel, G. Montagnac, H. Cardon, D.A. Sverjensky. "In situ Raman Study and

489   Thermodynamic Model of Aqueous Carbonate Speciation in Equilibrium with Aragonite

490   under Subduction Zone Conditions". GCA. 2014. 132: 375–390.

491   39. B.G. Oliver, A.R. Davis. "Vibrational Spectroscopic Studies of Aqueous Alkali Metal

492   Bicarbonate and Carbonate Solutions". Can. J. Chem. 1973. 51(5): 698–702.

493   40. W.W. Rudolph, D. Fischer, G. Irmer. "Vibrational Spectroscopic Studies and Density

494   Functional Theory Calculations of Speciation in the CO_2 —Water System". Appl.

495   Spectrosc. 2006. 60(2): 130–144.

496   41. W.W. Rudolph, G. Irmer, E. Königsberger. "Speciation Studies in Aqueous HCO_3^-–

497   CO_3^{2-} Solutions. A Combined Raman Spectroscopic and Thermodynamic Study". Dalton

498   Trans. RSC. 2008. (7): 900–908.

499   42. M.-C. Caumon, A. Tarantola, R. Mosser-Ruck. "Raman Spectra of Water in Fluid

500   Inclusions: I. Effect of Host Mineral Birefringence on Salinity Measurement". J. Raman

501   Spectrosc. 2015. 46(10): 969–976.

502   43. J.D. Frantz. "Raman Spectra of Potassium Carbonate and Bicarbonate Aqueous Fluids at

503   Elevated Temperatures and Pressures: Comparison with Theoretical Simulations". Chem.

504   Geol. 1998. 152(3): 211–225.

505   44. J. Wu, H. Zheng. "Quantitative Measurement of the Concentration of Sodium Carbonate

506   in the System of Na_2CO_3–H_2O by Raman Spectroscopy". Chem. Geol. 2010. 273(3): 267–

507   271.

508   45. Q. Sun, C. Qin. "Raman OH Stretching Band of Water as an Internal Standard to

509   Determine Carbonate Concentrations". Chem. Geol. 2011. 283(3): 274–278.

510   46. K.E. Chave. "Evidence on History of Sea Water from Chemistry of Deeper Subsurface

511   Waters of Ancient Basins". Am. Assoc. Pet. Geol. Bull. 1960. 44(3): 357–370.

512   47. F.T. Mackenzie, R.M. Garrels. "Chemical Mass Balance Between Rivers and Oceans".

513   Am. J. Sci. 1966. 264(7): 507–525.

514   48. R.M. Garrels, F. Mackenzie. "Origin of the Chemical Compositions of Some Springs and

515   Lakes". Am. Chem. Soc. Adv. Chem. Ser. 1967. Pp. 222–242.

516   49. S.D. Burley, J. Mullis, A. Matter. "Timing Diagenesis in the Tartan Reservoir (UK North

517   Sea): Constraints from Combined Cathodoluminescence Microscopy and Fluid Inclusion

518   Studies". Mar. and Petrol. Geol. 1989. 6(2): 98–120.

519   50. W. Stumm, J.J. Morgan. Aquatic Chemistry: Chemical Equilibria and Rates in Natural

520   Waters. Wiley, New York, NY, 1996. Pp. 1-1022.

521   51. D. Langmuir. Aqueous Environmental Geochemistry. 1st edition. Prentice Hall, Upper

522   Saddle River, NJ, 1997. Pp. 1-602

523   52. M.E. Sumner. Handbook of Soil Science. 1st edition. CRC Press, Boca Raton, Fla, 1999.

524   Pp. 1-843.

525   53. F.J. Millero, T.B. Graham, F. Huang, H. Bustos-Serrano, D. Pierrot. "Dissociation

526   Constants of Carbonic Acid in Seawater as a Function of Salinity and Temperature". Mar.

527   Chem. 2006. 100(1): 80–94.

528   54. K. Onda, E. Sada, T. Kobayashi, S. Kito, K. Ito. "Salting-Out Parameters of Gas

529   Solubility in Aqueous Salt Solutions". JCEJ. 1970. 3(1): 18–24.

530   55. J.N. Butler. Ionic Equilibrium: Solubility and pH Calculations. John Wiley & Sons, New

531   York, NY, 1998. Pp. 1-559.

532   56. J.I. Drever. The Geochemistry of Natural Waters: Surface and Groundwater

533   Environments. Prentice Hall, Hoboken, NJ, 1997. Pp. 1-436.

534   57. T. Dieing, O. Hollricher. "High-Resolution, High-Speed Confocal Raman Imaging". Vib.

535   Spectrosc. 2008. 48(1): 22–27.

536   58. A.R. Davis, B.G. Oliver. "A Vibrational-Spectroscopic Study of the Species Present in the

537   CO_2-H_2O System". J. Solution Chem. 1972. 1(4): 11.

538   59. J.D. Pasteris, O. Beyssac. "Welcome to Raman Spectroscopy: Successes, Challenges, and

539   Pitfalls". Elements. 2020. 16(2): 87–92.

540   60. G. Giridhar, R.R.K.N. Manepalli, G. Apparao. "Confocal Raman Spectroscopy". In: S.

541   Thomas, R. Thomas, A.K. Zachariah, editors. Spectroscopic Methods for Nanomaterials

542   Characterization. Elsevier, Amsterdam, NL, 2017. Chap. 7. Pp. 141–161.

543   61. R.H. Goldstein. "Petrographic Analysis of Fluid Inclusions". In: I. Samson, A. Anderson,

544   D. Marshall, editors. Fluid Inclusions: Analysis and Interpretation. Mineral. Assoc.

545   Canada, Quebec City, QC, 2003. Vol. 32. Chap. 2. Pp. 1-43.

546   62. K.M. Rosso, R.J. Bodnar. "Microthermometric and Raman Spectroscopic Detection

547   Limits of CO_2 in Fluid Inclusions and the Raman Spectroscopic Characterization of CO_2".

548   GCA. 1995. 59(19): 3961–3975.

549   63. Y. Kawakami, J. Yamamoto, H. Kagi. "Micro-Raman Densimeter for CO_2 Inclusions in

550   Mantle-Derived Minerals". Appl. Spectrosc. 2003. 57(11): 1333–1339.

551   64. X. Wang, W. Hu, I.-M. Chou. "Raman Spectroscopic Characterization on the OH

552   Stretching Bands in NaCl–Na_2CO_3–Na_2SO_4–CO_2–H_2O systems: Implications for the

553   Measurement of Chloride Concentrations in Fluid Inclusions". J. Geochem. Explor. 2013.

554   132: 111–119.

555   65. J.J. Carroll, J.D. Slupsky, A.E. Mather. "The Solubility of Carbon Dioxide in Water at

556   Low Pressure". J. Phys. Chem. Ref. Data. 1991. 20(6): 1201–1209.

557   66. R. Wiebe, V.L. Gaddy. "The Solubility of Carbon Dioxide in Water at Various

558   Temperatures from 12 to 40° and at Pressures to 500 Atmospheres. Critical Phenomena".

559   J. Am. Chem. Soc. 1940. 62(4): 815–817.

560   67. R.E. Zeebe, D. Wolf-Gladrow. "CO_2 in Seawater: Equilibrium, Kinetics, Isotopes".

561   Elsevier Oceanography Series, Amsterdam, NL. 2001. Vol. 65. Pp. 1-346.

562   68. M.J. Pelletier. Analytical Applications of Raman Spectroscopy. Blackwell Publishing,

563   Malden, MA. 1999. Pp. 1-478.

564

565

566

567

568

569

570

571

572

573

574

575

576

577

578

579

580

581

582

Figures and Tables
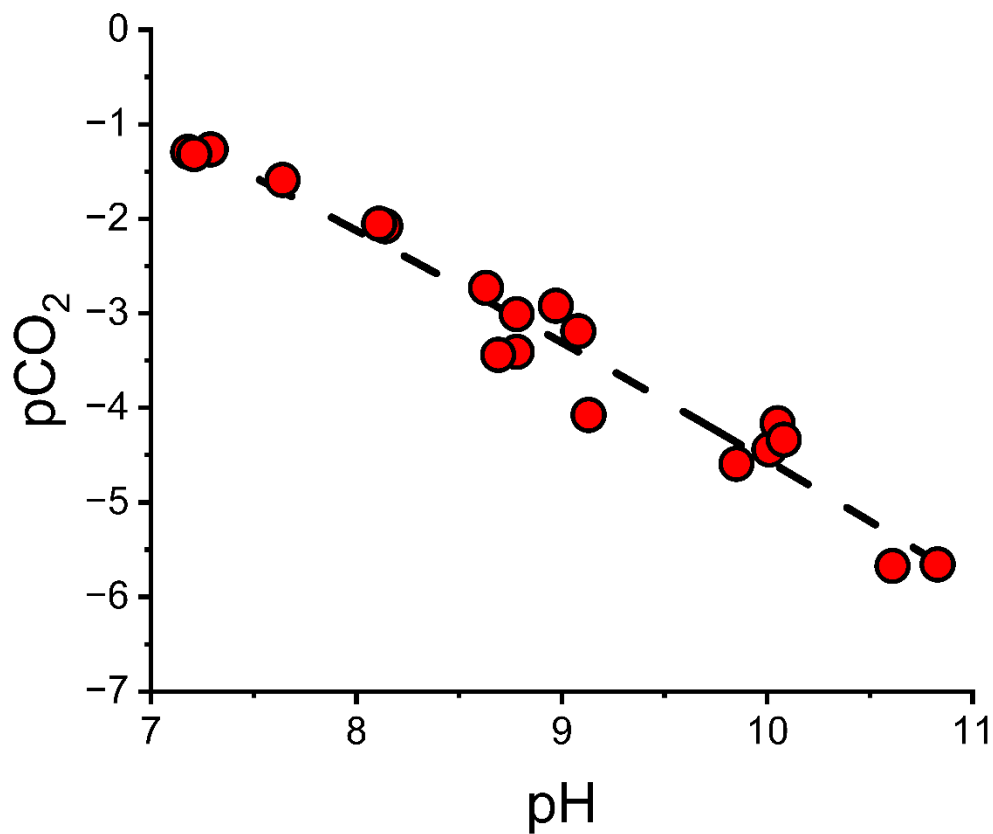
585 **Figure 1.** The relationship between pH and pCO_2 calculated from the stock solutions show that

586 they can be used to calibrate over a wide range of CO_2 concentrations.

587

588

589

590

591

592
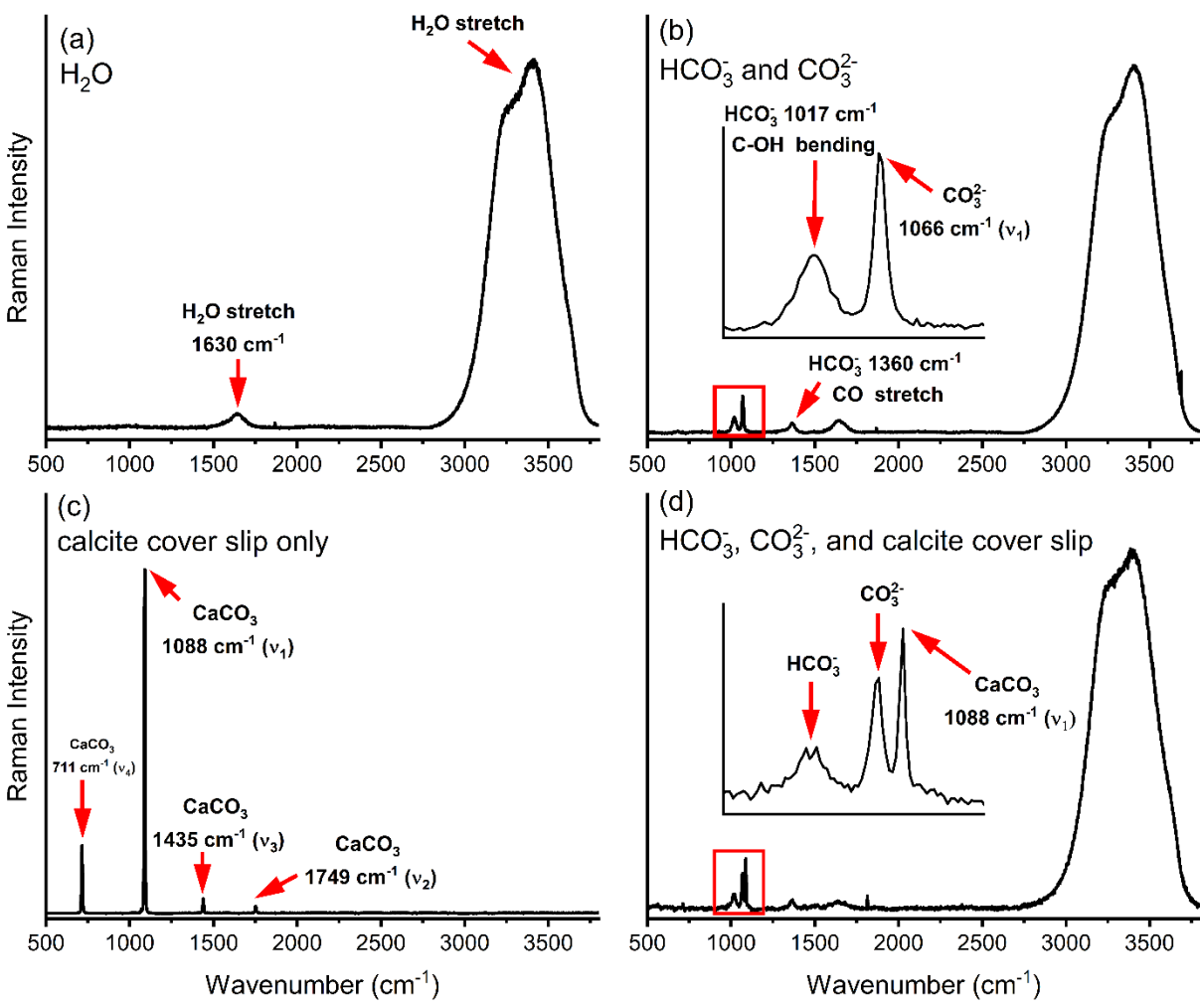
Figure 2. Background corrected Raman spectra of the different components used to construct the calibration curves. (a) Raman spectra of the Millipore water used to make the solutions. (b) Raman spectra of a 0.15 molar $NaHCO_3$ and 0.03 molar Na_2CO_3 solution; inset expands area of the red box between 950 – 1150 cm^{-1}. The main HCO_3^- and CO_3^{2-} bands are ~1017 and ~1066 cm^{-1}, respectively. (c) Raman spectra of the calcite cover slip with the main $CaCO_3$ band at ~1088 cm^{-1}. (d) Raman spectra of the 0.15 molar $NaHCO_3$ and 0.03 molar Na_2CO_3 solution with the Raman focused 100 μm below the calcite cover slip; inset that shows positions of the HCO_3^-, CO_3^{2-}, and $CaCO_3$ bands. Abbreviations: v_1, symmetric stretching vibration; v_2, out-of-plane bending vibration; v_3, antisymmetric stretching vibration; v_4, in-plane bending vibration.

28

603
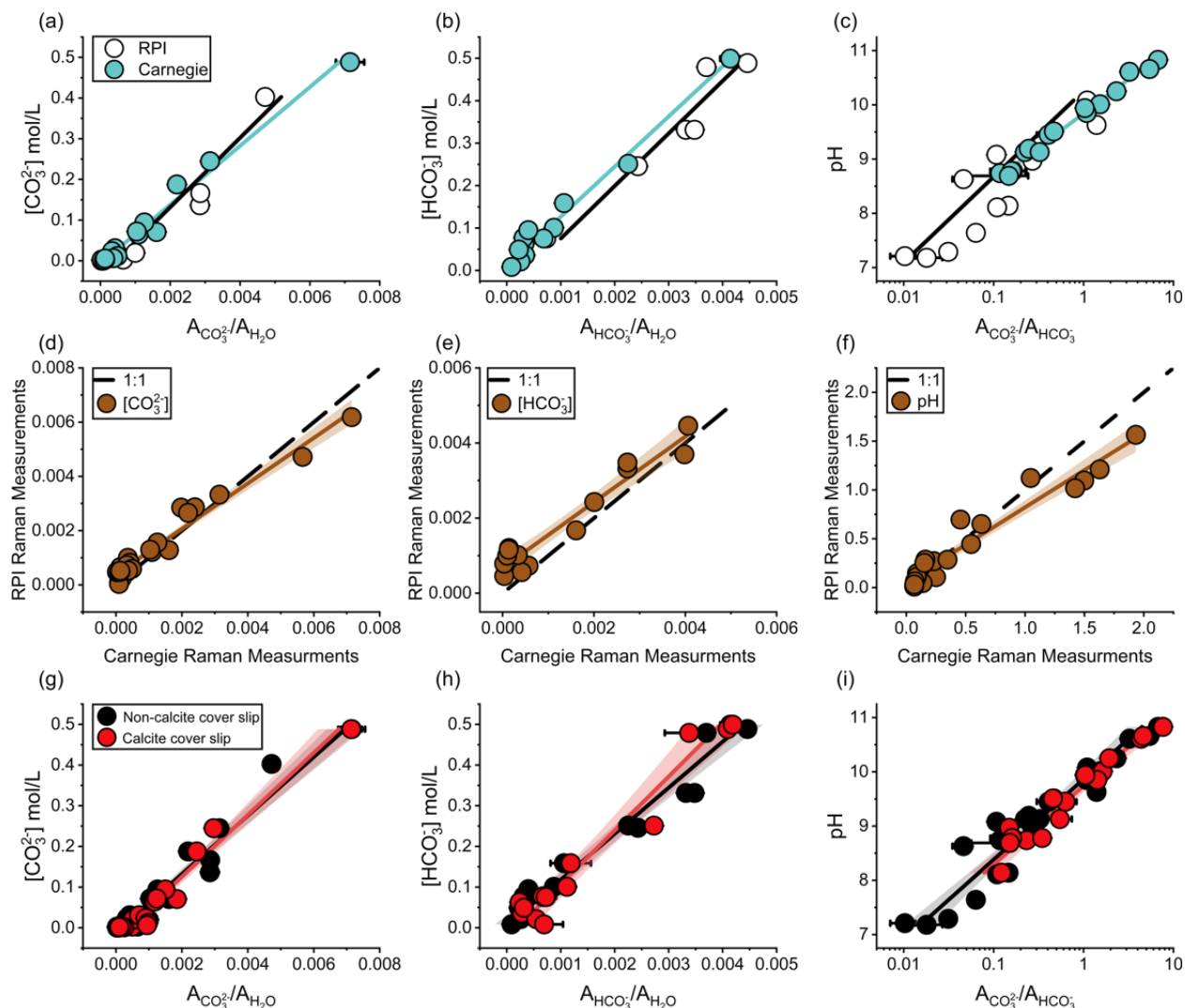
Figure 3. (a), (b), and (c) show the response of the two instruments used in this study to quantify $[CO_3^{2-}]$, $[HCO_3^-]$, and pH, respectively. Rensselaer Polytechnic Institute (RPI) is in white, and Carnegie Institute of Science (Carnegie) is in blue. $[CO_3^{2-}]$ (a) and $[HCO_3^-]$ (b) data comparisons show a linear relationship when the area of the CO_3^{2-} and HCO_3^- bands are ratioed with the water band. The pH (c) response shows a linear relationship when the area of the CO_3^{2-} and HCO_3^- bands are ratioed. Note the logarithmic scale of the x-axis in panel C. Measurements made at Carnegie and RPI are compared between $[CO_3^{2-}]$ (d), $[HCO_3^-]$ (e), and pH (f). Notice the near 1:1 agreement between $[CO_3^{2-}]$. However, pH and $[HCO_3^-]$ deviate slightly from a 1:1, possibly due

612   to slight differences in laser output between the two instruments. G-I are the comparisons of

613   carbonate species concentrations and pH solution calibrations with (red) and without (black) the

614   calcite cover slip. Calibration solutions of $[CO_3^{2-}]$ (g) and $[HCO_3^-]$ (h) show a linear relationship

615   when the area of CO_3^{2-} and HCO_3^- bands are ratioed to the water band. pH (i) solution calibration

616   shows a linear relationship when the area of the CO_3^{2-} and HCO_3^- bands are ratioed to each other.

617   Note the logarithmic scale of the x-axis in panel (i). 95% confidence intervals are the colored

618   shaded areas. Concentrations are in mol/L.

619

620

621

622

623

624

625

626

627

628

629

630
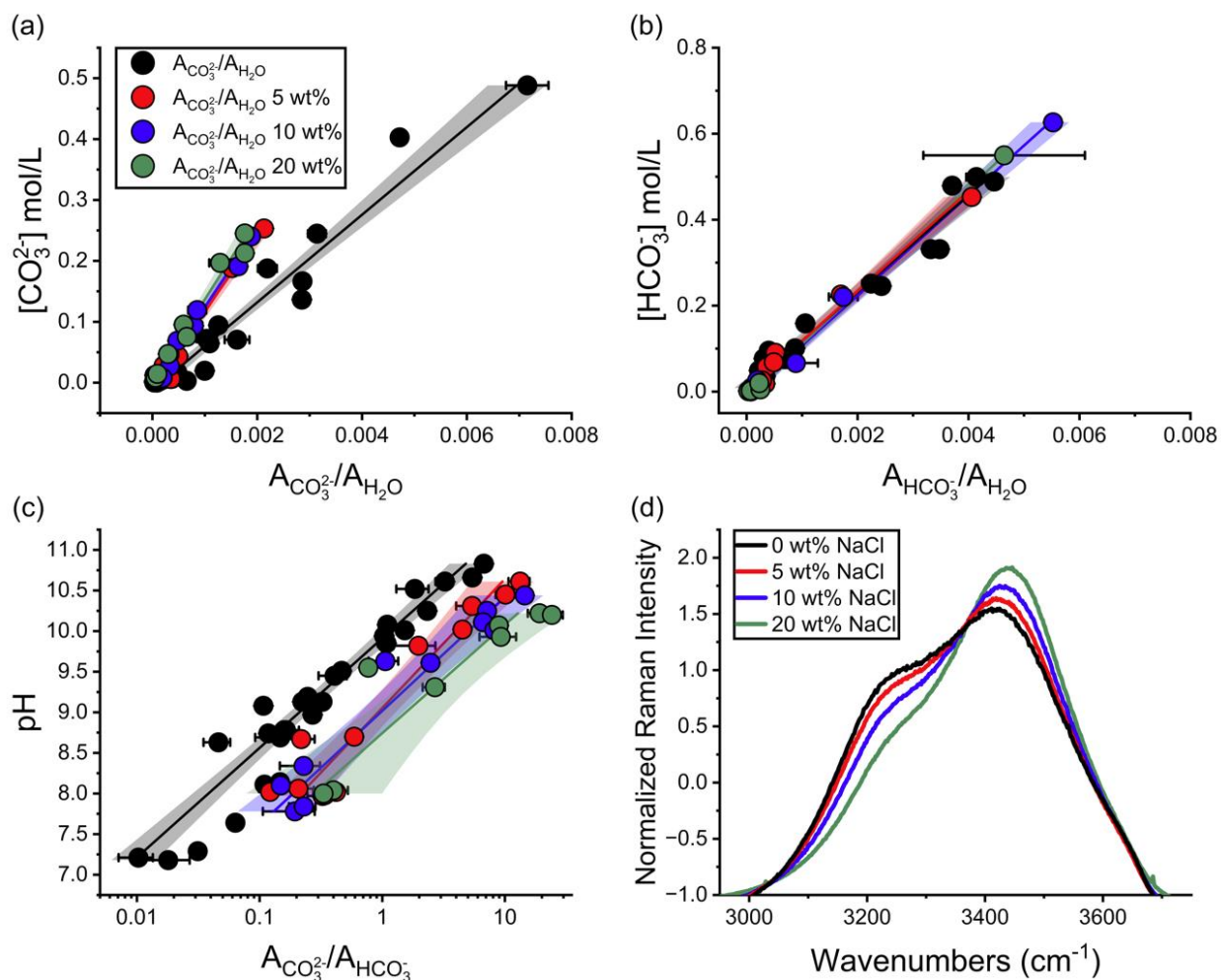
Figure 4. Comparisons of carbonate species concentrations (CO_3^{2-} and HCO_3^-) and pH solution

calibrations at various NaCl concentrations (salinities). Linear solution calibration relationship of

[CO_3^{2-}] (a) and [HCO_3^-] (b) are shown versus the area ratio of CO_3^{2-} and HCO_3^- bands with the

water band. Linear pH (c) solution calibration relationship versus the area ratio between the

CO_3^{2-} and HCO_3^- bands. Note the logarithmic scale of the x-axis in panel (c). 95% confidence

intervals are the color shaded areas. Normalized Raman OH^- stretch at different NaCl

concentrations (d). Concentrations are in mol/L.
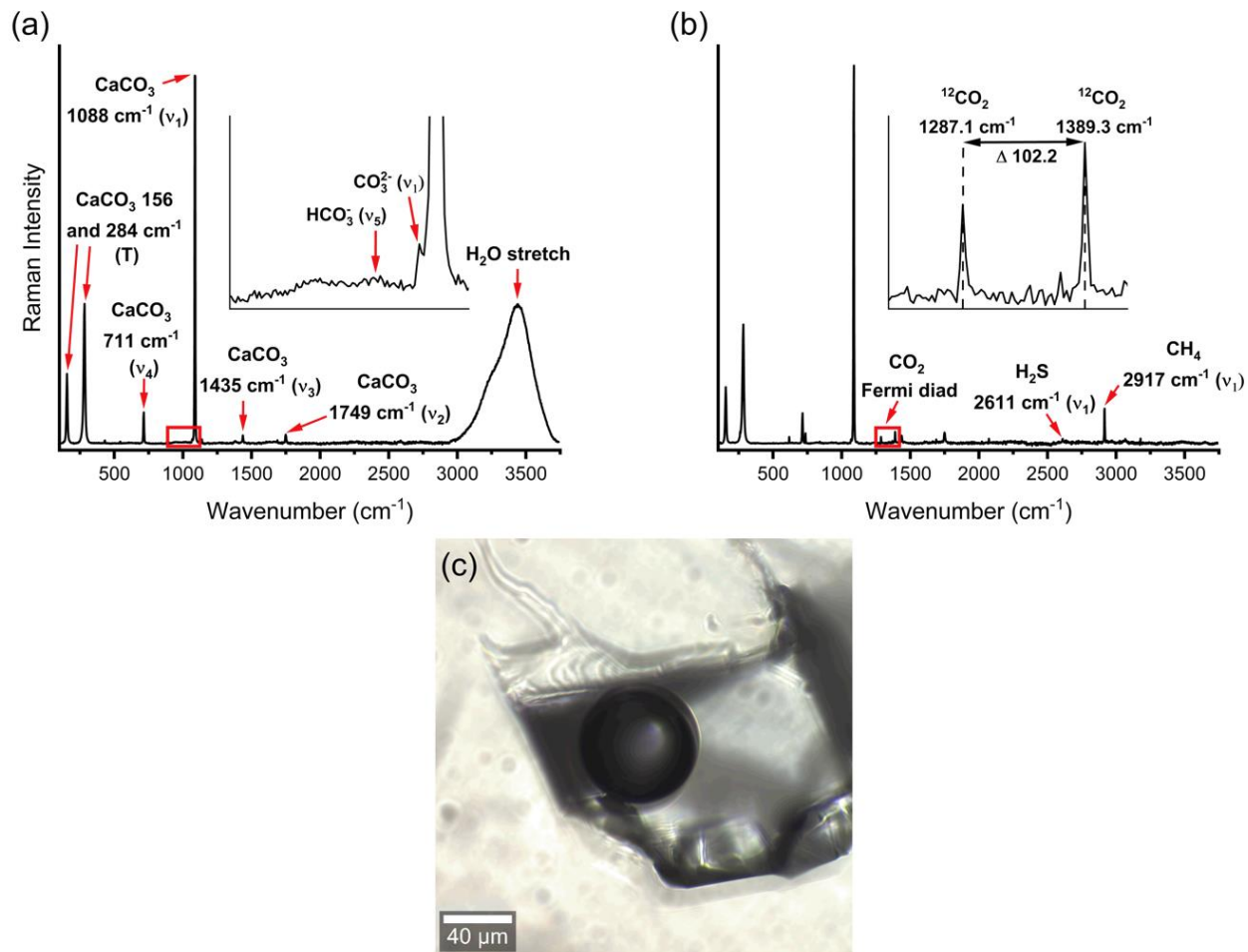
Figure 5. Example Raman spectra of the liquid (a) and gas phase (b) of the large fluid inclusion measured in this study. Liquid phase showing HCO_3^- (1017 cm^{-1}), CO_3^{2-} (1066 cm^{-1}), and H_2O (1630 and 2750-3750 cm^{-1}) bands with an inset of the red box for the HCO_3^- and CO_3^{2-} bands. Gas phase shows the CO_2 Fermi diad (1285 and 1388 cm^{-1}), hydrogen sulfide (2611 cm^{-1}), and methane (2917 cm^{-1}). Gas phase inset of the red box shows the CO_2 Fermi diad and the difference between band distance (Δ) estimates fluid density. Host mineral calcite bands are present in both in liquid and gas phase spectra at (156, 284, 711, 1088, and 1435 cm^{-1}). Photomicrograph of the analyzed fluid inclusion in Iceland Spar (c). Abbreviations: T, translational lattice; ν_1, symmetric stretching vibration; ν_2, out-of-plane bending vibration; ν_3, antisymmetric stretching vibration; ν_4, in-plane bending vibration.

650   **Table I.** Range of carbonate and bicarbonate concentrations (mol/L), and pH in natural waters.

Environment	[CO_3^{2-}]	[HCO_3^-]	pH	Reference
Oceans	0.0002 - 0.0003	0.002 - 0.03	7.4 - 8.3	36,46–48
Rivers	3.6x10^-8	0.0005 - 0.002	5.28 - 8.5	36,47,50,69
Groundwater	0.00169	0.0001 - 0.003	5.1 – 10.7	51,52,69
Soil	-	0.0001 - 0.003	4.8 - 10.02	51,52
Fluid Inclusions	-	0.007 - 0.014	-	49

651

652

653

654

655

656

657

658

659

660

661

662

663

664

665

666

667

668

Table II. Solutions and associated area ratio of carbonate species to water, with and without the calcite cover slip, measured using

Confocal Raman spectroscopy.

671

Institution	NaCl wt%	$[CO_3^{2-}]$	$[HCO_3^-]$	pH	A_{CO3}/A_{H2O} non-CCS	A_{HCO3}/A_{H2O} non-CCS	A_{CO3}/A_{HCO3} non-CCS	A_{CO3}/A_{H2O} CCS	A_{HCO3}/A_{H2O} CCS	A_{CO3}/A_{HCO3} CCS
Carnegie	0	0.4883	0.0155	11.87	0.00715	-	-	0.00714	-	-
Carnegie	0	0.24473	0.00951	11.78	0.00314	-	-	0.00296	-	-
Carnegie	0	0.0943	0.00555	11.6	0.00126	-	-	0.0015	-	-
Carnegie	0	0.0719	0.00497	11.53	0.00104	-	-	0.00124	-	-
Carnegie	0	0.1876	0.063	10.83	0.00219	3.29E-04	6.72863	0.00245	2.38E-04	7.63803
Carnegie	0	0.0646	0.0361	10.61	0.00109	3.41E-04	3.24354	0.00118	2.82E-04	4.37463
Carnegie	0	0.0309	0.0212	10.52	4.20E-04	2.54E-04	1.84181	7.02E-04	5.48E-04	1.26751
RPI	0	0.13647	0.24578	10.08	0.00285	0.00243	1.09603	-	-	-
Carnegie	0	0.0706	0.1588	10.01	0.00161	0.00106	1.52427	0.00185	0.00119	1.62867
Carnegie	0	0.0235	0.0772	9.85	3.34E-04	3.11E-04	1.08225	9.02E-04	6.63E-04	1.42146
Carnegie	0	0.0011	0.0084	9.45	3.47E-05	8.86E-05	0.40751	2.52E-04	6.91E-04	0.63242
Carnegie	0	0.0028	0.0492	9.13	3.45E-05	2.25E-04	0.22325	1.70E-04	3.17E-04	0.54556
RPI	0	0.0055	0.0951	9.13	1.33E-04	3.99E-04	0.32558			
RPI	0	0.01958	0.47922	8.97	9.97E-04	0.0037	0.26982	5.06E-04	0.00338	0.14911
Carnegie	0	0.0064	0.2512	8.78	3.73E-04	0.00225	0.16409	9.45E-04	0.00273	0.34698
Carnegie	0	0.0026	0.1007	8.78	1.38E-04	8.73E-04	0.1588	1.80E-04	0.00111	0.16044
Carnegie	0	0.0117	0.4992	8.74	4.88E-04	0.00414	0.11785	9.74E-04	0.00419	0.23305
Carnegie	0	0.0016	0.0755	8.69	9.89E-05	6.83E-04	0.14744	1.04E-04	7.22E-04	0.15116
RPI	0	0.003	0.4887	8.14	6.54E-04	0.00446	0.14648	5.02E-04	0.00409	0.12254
RPI	0	0.0027	0.4883	8.11	-	-	0.10951	-	-	-
RPI	0	8.99E-04	0.47353	7.64	-	-	0.06345	-	-	-
RPI	0	3.78E-04	0.44574	7.29	-	-	0.0313	-	-	-
RPI	0	2.31E-04	0.33151	7.21	3.57E-05	0.00348	0.01028	-	-	-
RPI	0	2.21E-04	0.33151	7.18	8.24E-05	0.00332	0.01798	-	-	-

Carnegie	5	0.25316	0.00595	10.61	0.00213	1.66E-04	13.28998	-	-	-
Carnegie	5	0.09175	0.00318	10.45	7.71E-04	7.83E-05	10.10648	-	-	-
Carnegie	5	0.04661	0.00224	10.31	3.86E-04	7.41E-05	5.38911	-	-	-
Carnegie	5	0.18816	0.01853	10.02	0.00152	3.38E-04	4.50271	-	-	-
Carnegie	5	0.00884	0.00129	9.82	6.40E-05	3.37E-05	1.96885	-	-	-
Carnegie	5	0.02801	0.05785	8.7	2.13E-04	3.63E-04	0.59025	-	-	-
Carnegie	5	0.01162	0.0261	8.67	6.02E-05	2.79E-04	0.21847	-	-	-
RPI	5	0.02255	0.22562	8.06	3.46E-04	0.0017	0.20726	-	-	-
RPI	5	0.04324	0.4528	8.02	4.95E-04	0.00406	0.12176	-	-	-
RPI	5	0.00884	0.09038	8.02	2.14E-04	5.17E-04	0.41969	-	-	-
RPI	5	0.00605	0.0683	7.98	3.52E-04	4.90E-04	0.3404	-	-	-
RPI	5	-	-	7.97	0.00116	0.00357	0.32589	-	-	-
Carnegie	10	0.24019	0.00423	10.44	0.00188	1.31E-04	14.48862	-	-	-
Carnegie	10	0.09348	0.00253	10.25	7.91E-04	1.01E-04	7.14797	-	-	-
Carnegie	10	0.04655	0.00174	10.11	3.25E-04	3.13E-05	6.6306	-	-	-
Carnegie	10	0.19119	0.00953	10.01	0.00164	2.03E-04	8.1797	-	-	-
Carnegie	10	0.00824	9.26E-04	9.63	1.72E-04	-	1.05972	-	-	-
Carnegie	10	0.06884	0.00841	9.61	4.76E-04	1.94E-04	2.47359	-	-	-
Carnegie	10	0.01219	0.02638	8.34	4.05E-05	1.94E-04	0.22844	-	-	-
RPI	10	-	-	8.1	5.69E-04	0.00383	0.14883	-	-	-
RPI	10	0.11916	0.62652	8	8.54E-04	0.00552		-	-	-
RPI	10	0.00775	0.06657	7.84	1.93E-04	8.89E-04	0.22931	-	-	-
RPI	10	0.02702	0.22046	7.78	3.31E-04	0.00174	0.19389	-	-	-
Carnegie	20	0.24511	0.00219	10.22	0.00176	9.51E-05	19.13996	-	-	-
Carnegie	20	0.21278	0.00217	10.2	0.00176	7.61E-05	24.13153	-	-	-
Carnegie	20	0.09528	0.00134	10.07	5.94E-04	6.87E-05	8.92398	-	-	-
Carnegie	20	0.04701	9.02E-04	9.93	2.95E-04	3.38E-05	9.26285	-	-	-
Carnegie	20	0.00822	4.02E-04	9.55	5.91E-05	7.71E-05	0.76925	-	-	-
Carnegie	20	0.07532	0.00535	9.31	6.56E-04	2.49E-04	2.68553	-	-	-
Carnegie	20	0.01445	0.01975	8.04	9.38E-05	2.28E-04	0.40004	-	-	-
RPI	20	0.19684	0.54965	8	0.00129	0.00464	0.33187	-	-	-

672

673

674 **Table III.** Results of $[CO_3^{2-}]$ and $[HCO_3^-]$ estimation correlations with and without the calcite

675 cover slip.

	Test	Equation	R^2	95% CI
Non-calcite cover slip	$[CO_3^{2-}]$	$y = 73.12x - 0.013$	0.96	0.01
	$[HCO_3^-]$	$y = 107.30x + 0.015$	0.97	0.0002
	pH	$y = 1.362x + 9.724$	0.97	0.05
Calcite cover slip	$[CO_3^{2-}]$	$y = 73.52x - 0.024$	0.96	0.01
	$[HCO_3^-]$	$y = 123.63x - 0.014$	0.97	0.0002
	pH	$y = 1.365x + 9.803$	0.96	0.06

676

677

678

679

680

681

682

683

684

685

686

687

688

689

690

691

692

693

694

695

696

697

698

699

700

701

702

703

704

Table IV. Results of $[CO_3^{2-}]$, $[HCO_3^-]$, and pH estimation correlations at different NaCl wt%.

Test	NaCl wt%	Equation	R^2	95% CI
[CO₃²⁻]	5 wt%	$y = 131.4x + 0.005$	0.97	0.02
	10 wt%	$y = 124.6x - 0.009$	0.98	0.02
	20 wt%	$y = 126.5x - 0.003$	0.98	0.02
[HCO₃⁻]	5 wt%	$y = 114.7 + 0.002$	0.99	0.02
	10 wt%	$y = 115.7x - 0.009$	0.99	0.01
	20 wt%	$y = 120.4x - 0.009$	0.99	0.01
pH	5 wt%	$y = 1.45x + 9.05$	0.92	0.3
	10 wt%	$y = 1.31x + 9.03$	0.94	0.2
	20 wt%	$y = 1.11x + 8.86$	0.83	0.4

Table V. Estimated CO_3^{2-} and HCO_3^- concentrations (mol/L), pH, pCO_2, and CO_2 (ppm) of the calcite fluid inclusion.

[CO₃²⁻]	[HCO₃⁻]	pH	pCO₂	CO₂ (ppm)
0.11 ± 0.03	0.17 ± 0.05	10.1 ± 0.19	-2.75 ± 0.29	2217 ± 1319